

# Effect of shear, compaction and nesting on permeability of the orthogonal plain-weave fabric preforms

M. Grujicic<sup>a,\*</sup>, K.M. Chittajallu<sup>a</sup>, Shawn Walsh<sup>b</sup>

<sup>a</sup> Department of Mechanical Engineering, Clemson University, 241 Engineering Innovation Building, Clemson, SC 29634, USA

<sup>b</sup> Army Research Laboratory—WMD AMSRL-WM-MD, Proving Ground, Aberdeen, MD 21005-5069, USA

Received 10 October 2003; received in revised form 9 March 2004; accepted 26 March 2004

## Abstract

Permeability of fabric preforms and its changes due to various modes of the fabric distortion or deformation as well due to fabric layers shifting and compacting is one of the key factors controlling infiltration of the preforms with resin within the common polymer-matrix composite liquid-molding fabrication processes. While direct measurements of the fabric permeability generally yield the most reliable results, a large number of the fabric architectures used and numerous deformation and layers rearrangement modes necessitates the development and the use of computational models for the prediction of preform permeability. One such model, the so-called lubrication model, is adapted in the present work to study the effect of the mold walls, the compaction pressure, the fabric-tows shearing and the fabric layers shifting on permeability of the preforms based on orthogonal balanced plain-weave fabrics. The model predictions are compared with their respective experimental counterparts available in the literature and a reasonably good agreement is found between the corresponding sets of results.

© 2004 Elsevier B.V. All rights reserved.

## 1. Introduction

Over the last two decades, processing of high-performance polymer-matrix composites via the use of modern resin-injection technologies has made major advances and expanded from its aerospace roots to military and diverse civil applications. At the same time, processing science has become an integral part of the composite-manufacturing technology so that empiricism and semi-empiricism have given way to greater use of computer modeling and simulations of the fabrication processes. Among the modern polymer-matrix composite manufacturing techniques, liquid-molding processes such as resin transfer molding (RTM), vacuum assisted resin transfer molding (VARTM) and structural reaction injection molding (SRIM) have a prominent place. A detailed review of the major liquid molding processes can be found in the recent work of Lee [1]. One common feature to all these composite fabrication processes is the use of low-pressure infiltration of the porous fabric preforms with a viscous fluid (resin). Conformation of the fabric preforms to the ridges and recesses in the mold and the applied pressure can induce significant

distortions and deformations in the fabric as well as give rise to shifting of the individual fabric layers and, in turn, cause significant change in local permeability of the preform. Since the infiltrating fluid follows the path of least resistance, local changes in the fabric permeability can have a great influence on the mold filling process influencing the filling time, the filling completeness and the formation of pores and dry spots. Hence, the knowledge of the effect of various distortion, shearing and shifting modes on the fabric permeability is a critical step toward better designs and control of the liquid molding processes.

Permeability of a porous medium is one of the most important parameters controlling the flow of a fluid through such medium. In simple terms, permeability can be defined as a (tensorial) quantity which relates the local velocity vector of the fluid flow with the associated pressure gradient. In polymer-matrix composite liquid-molding manufacturing processes (e.g. in the RTM and the VARTM processes), the porous medium consists of woven- or weaved-fabric preforms placed in the mold and the fluid flow of interest involves preform infiltration with resin. Complete infiltration of the preform with resin is critical for obtaining high-integrity, high-quality composite structures. The knowledge of the preform permeability and its changes due to fabric bending, shearing, compression, shifting, etc.

\* Corresponding author. Tel.: +1-864-656-5639; fax: +1-864-656-4435.  
E-mail address: [mica.grujicic@ces.clemson.edu](mailto:mica.grujicic@ces.clemson.edu) (M. Grujicic).

## Report Documentation Page

*Form Approved*  
*OMB No. 0704-0188*

Public reporting burden for the collection of information is estimated to average 1 hour per response, including the time for reviewing instructions, searching existing data sources, gathering and maintaining the data needed, and completing and reviewing the collection of information. Send comments regarding this burden estimate or any other aspect of this collection of information, including suggestions for reducing this burden, to Washington Headquarters Services, Directorate for Information Operations and Reports, 1215 Jefferson Davis Highway, Suite 1204, Arlington VA 22202-4302. Respondents should be aware that notwithstanding any other provision of law, no person shall be subject to a penalty for failing to comply with a collection of information if it does not display a currently valid OMB control number.

1. REPORT DATE <b>2004</b>	2. REPORT TYPE	3. DATES COVERED <b>00-00-2004 to 00-00-2004</b>	
4. TITLE AND SUBTITLE <b>Effect of shear, compaction and nesting on permeability of the orthogonal plain-weave fabric preforms</b>		5a. CONTRACT NUMBER	
		5b. GRANT NUMBER	
		5c. PROGRAM ELEMENT NUMBER	
6. AUTHOR(S)		5d. PROJECT NUMBER	
		5e. TASK NUMBER	
		5f. WORK UNIT NUMBER	
7. PERFORMING ORGANIZATION NAME(S) AND ADDRESS(ES) <b>Celmsn University, Department of Mechanical Engineering, Clemson, SC, 29634</b>		8. PERFORMING ORGANIZATION REPORT NUMBER	
9. SPONSORING/MONITORING AGENCY NAME(S) AND ADDRESS(ES)		10. SPONSOR/MONITOR'S ACRONYM(S)	
		11. SPONSOR/MONITOR'S REPORT NUMBER(S)	
12. DISTRIBUTION/AVAILABILITY STATEMENT <b>Approved for public release; distribution unlimited</b>			
13. SUPPLEMENTARY NOTES			
14. ABSTRACT <b>Permeability of fabric preforms and its changes due to various modes of the fabric distortion or deformation as well due to fabric layers shifting and compacting is one of the key factors controlling infiltration of the preforms with resin within the common polymer-matrix composite liquid-molding fabrication processes. While direct measurements of the fabric permeability generally yield the most reliable results, a large number of the fabric architectures used and numerous deformation and layers rearrangement modes necessitates the development and the use of computational models for the prediction of preform permeability. One such model, the so-called lubrication model, is adapted in the present work to study the effect of the mold walls, the compaction pressure, the fabric-tows shearing and the fabric layers shifting on permeability of the preforms based on orthogonal balanced plain-weave fabrics. The model predictions are compared with their respective experimental counterparts available in the literature and a reasonably good agreement is found between the corresponding sets of results.</b>			
15. SUBJECT TERMS			
16. SECURITY CLASSIFICATION OF:			17. LIMITATION OF ABSTRACT
a. REPORT <b>unclassified</b>	b. ABSTRACT <b>unclassified</b>	c. THIS PAGE <b>unclassified</b>	<b>Same as Report (SAR)</b>
			18. NUMBER OF PAGES <b>12</b>
			19a. NAME OF RESPONSIBLE PERSON

**Nomenclature**

$f$	fiber volume fraction
$h$	fabric thickness (m)
$K$	permeability tensor of the fabric ( $\text{m}^2$ )
$L$	length of the quarter unit cell (m)
$p$	pressure (Pa)
$r$	fiber radius (m)
$s$	relative shift of the adjacent fabric layers (m)
$u$	$x$ -component of the resin velocity ( $\text{m s}^{-1}$ )
$U$	in-plane resin velocity magnitude ( $\text{m s}^{-1}$ )
$v$	$y$ -component of the resin velocity ( $\text{m s}^{-1}$ )
$w$	$z$ -component of the resin velocity ( $\text{m s}^{-1}$ )
$W$	transverse resin velocity magnitude ( $\text{m s}^{-1}$ )

**Greek symbols**

$\eta$	resin viscosity ( $\text{N s m}^{-2}$ )
$\theta$	shear angle ( $^\circ$ )
$\phi$	relative dimensionless shift of the adjacent fabric layers

**Subscripts**

bot	quantity associated with the bottom surface of the fabric
corr	quantity corrected for the effect of shear on the fiber volume fraction
low	quantity associated with the lower mold surface
0	quantity associated with un-sheared fabric preform
top	quantity associated with the top surface of the fabric
upp	quantity associated with the upper mold surface
$\theta$	quantity associated with sheared fabric preform

**Superscripts**

B	quantity associated with the bottom channel
F	quantity associated with the fabric
T	quantity associated with the top channel

is crucial in the design of a composite fabrication process (e.g. in the design of the tool plate, or for placement of the resin injection ports). In general, the most accurate value of permeability of a porous medium is obtained by direct experimental measurements. However, the number of fabric architectures can be quite large and fabric distortion modes numerous making permeability determinations via the purely experimental means not a very appealing alternative. In addition, sometimes the experimentally determined permeability values reported by different researchers for the apparently identical fabric architectures can differ significantly. Consequently, significant effort has been invested

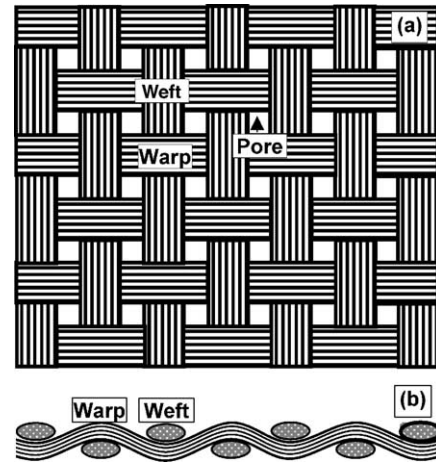


Fig. 1. A schematic of (a) the top view and (b) the edge view of a one-layer orthogonal plain-weave fabric preform.

over the past decade to develop computational tools which can be used, in conjunction with experimental measurements, to determine the preform permeability.

For the computational modeling approach to be successful in predicting permeability of the fabric preforms, it must include, in a correct way, both the actual architecture of the fabric and the basic physics of the flow through it. A schematic of the relatively simple orthogonal plain-weave one-layer fabric architecture is shown in Fig. 1. As seen in Fig. 1, the fabric consists of orthogonal (warp and weft) fiber yarns, which are woven together to form an interconnected network. Each yarn, on the other hand, represents a bundle of the individual fibers held together with thread. In addition, the fabric involves a network of empty pores and channels. When a fabric like the one shown in Fig. 1 is being infiltrated, the resin flows mainly through the pores and the channels. However, since the fabric tows are porous (pores and channel on a finer length scale exist between the fibers in tows), the resin also flows within the yarn. Thus when predicting the effective permeability of a fabric, the computational model must account for both components of the resin flow.

Prediction of the permeability of porous medium has been the subject of intense research for at least last two decades. Due to space limitations in this paper, it is not possible to discuss all the models proposed over this period of time. Nevertheless, one can attempt to classify the models. One such classification involves the following main types of models for permeability prediction in the porous media: (a) the phenomenological models based on the use of well established physical concepts such as the capillary flow, e.g. [2,3], or the lubrication flow, e.g. [4]. These models generally perform well within isotropic porous media with a simple architecture. (b) The numerical models which are based on numerical solutions of the governing differential equations. These models generally attempt to realistically represent the architecture of the fiber preform but, due to limitations in the computer speed and the memory size, are ultimately forced to the introduction of a number of major simplifications, e.g.

[5,6]. (c) The models which are based on a balance of the fabric architecture and the flow physics simplifications, enabling physically based predictions of the preform permeability within reasonably realistic fabric architectures. One of such models is the one proposed by Simacek and Advani [7]. The model of Simacek and Advani [7] also includes the effect of important factors such as: (a) the flow within the fiber yarn; (b) nesting in multi-layer fabric; and (c) distortion and deformation of the fabric. In the present work, the S model of Simacek and Advani [7] is extended to include the effect of shear of the fabric tows on the effective volume fraction of fibers.

The organization of the paper is as follows: a brief overview of the model proposed by Simacek and Advani [7] and its modifications are presented in Section 2. The application of their model to reveal the role of various fabric distortion and layers compaction phenomena is presented and discussed in Section 3. The main conclusions resulted from the present work are summarized in Section 4.

## 2. Computational procedure

### 2.1. Fabric architecture

In this work, only (un-sheared and sheared) balanced orthogonal plain-weave fabric is considered. Due to the in-plane periodicity, the fabric architecture can be represented using a unit cell. The entire orthogonal plain-weave fabric can then be obtained by repeating the unit cell in the in-plane ( $x$ - and  $y$ -directions). A schematic of one quarter of a plain-weave unit cell with the appropriate denotation for the system dimensions are shown in Fig. 2. In a typical plain-weave fabric, the fabric thickness ( $h$ ) to the quarter cell in-plane dimension ( $L$ ) ratio,  $h/L$ , is small (0.01–0.1), while the tow cross-section is nearly elliptical in shape with a large

(width-to-height) aspect ratio (5 or larger). The geometry of the tows within the cell can be described using various mathematical expressions, e.g. [8], for the top,  $z_{\text{top}}(x, y)$ , and the bottom,  $z_{\text{bot}}(x, y)$ , surfaces of the fabric, respectively. In the present work, the following sinusoidal functions originally proposed by Ito and Chou [9] are used:

$$z_{\text{top}}(x, y) = \frac{h}{2} \left( \sin \frac{2\pi}{L} x + \sin \frac{2\pi}{L} y \right) \quad (1)$$

$$z_{\text{bot}}(x, y) = -\frac{h}{2} \left( \sin \frac{2\pi}{L} x + \sin \frac{2\pi}{L} y \right) \quad (2)$$

As pointed out earlier, fiber tows have typically a near-elliptical cross-section and hence Eqs. (1) and (2) only approximate the actual tow cross-section shape. Nevertheless, they are used in the present work since they greatly simplify permeability calculations in the distorted fabric and are generally considered as a good approximation for the actual tow cross-section shape.

A simple examination of Fig. 2 shows that within a single-layer orthogonal plain-weave fabric unit cell, one can identify three distinct domains:

- the top channel, region T:  $z_{\text{top}} < z < h/2$ ;
- the fabric, region F:  $z_{\text{bot}} < z < z_{\text{top}}$ ;
- the bottom channel, region B:  $-h/2 < z < z_{\text{bot}}$ .

Regions T and B contain only the resin, while region F contains both the fiber tows and the resin. The resin flow through a unit cell is analyzed in the present paper by first considering the flow within the three regions separately and then utilizing the matching boundary conditions which ensure continuity in the pressure and the velocity components across the contact surfaces of the adjacent regions. The resin is considered as a Newtonian (constant density) fluid. The flows within the top and the bottom channels are assumed to be of a creeping nature (i.e. the inertial effects are neglected)

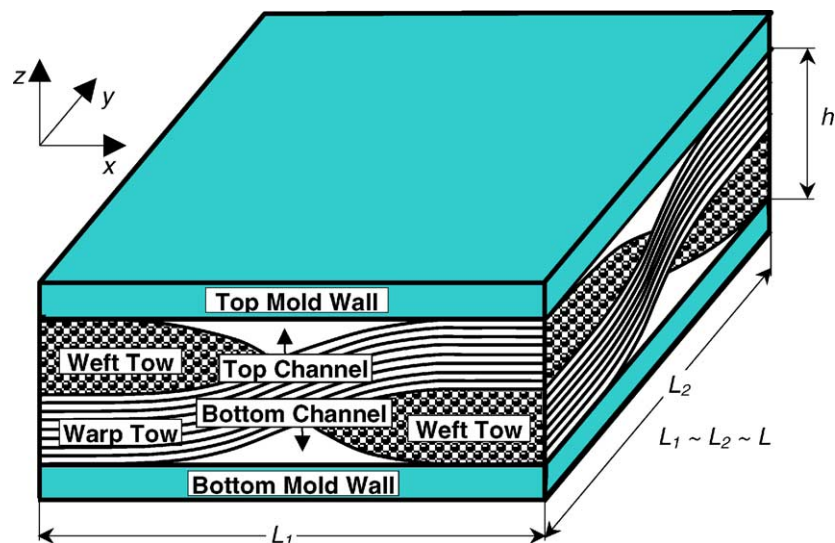


Fig. 2. Schematic of one quarter of the unit cell for a one-layer balanced orthogonal plain-weave fabric.

while the flow within the fabric is assumed to be governed by the Darcy's law (a velocity versus pressure gradient relation which eliminates the need for use of the momentum conservation equations).

## 2.2. Governing equations

### 2.2.1. Flow within the top and the bottom channels

Under typical fabric infiltration conditions, the resin flow within the regions T and B can be considered as a creeping flow in which inertial effects are negligibly small in comparison to the viscous effects. Under such conditions, at constant temperature, the resin flow can be described by the Stokes equations as:

$$-\frac{\partial p}{\partial x} + \eta \left( 2 \frac{\partial^2 u}{\partial x^2} + \frac{\partial^2 u}{\partial y^2} + \frac{\partial^2 u}{\partial z^2} + \frac{\partial^2 v}{\partial x \partial y} + \frac{\partial^2 w}{\partial x \partial z} \right) = 0 \quad (3)$$

$$-\frac{\partial p}{\partial y} + \eta \left( 2 \frac{\partial^2 v}{\partial y^2} + \frac{\partial^2 v}{\partial x^2} + \frac{\partial^2 v}{\partial z^2} + \frac{\partial^2 u}{\partial x \partial y} + \frac{\partial^2 w}{\partial y \partial z} \right) = 0 \quad (4)$$

$$-\frac{\partial p}{\partial z} + \eta \left( 2 \frac{\partial^2 w}{\partial z^2} + \frac{\partial^2 w}{\partial x^2} + \frac{\partial^2 w}{\partial y^2} + \frac{\partial^2 u}{\partial z \partial x} + \frac{\partial^2 v}{\partial y \partial z} \right) = 0 \quad (5)$$

$$\frac{\partial u}{\partial x} + \frac{\partial v}{\partial y} + \frac{\partial w}{\partial z} = 0 \quad (6)$$

where  $p$  is the pressure,  $u$ ,  $v$  and  $w$  are respectively the  $x$ -,  $y$ - and  $z$ -components of the resin velocity and  $\eta$  the resin viscosity.

Following the procedure of Simacek and Advani [7], which involves non-dimensionalization of the governing equations, and the use of the conditions:  $h/L \ll 1$  and  $WL/Uh \approx 1$  ( $U$  and  $W$  are (mean) in-plane and transverse resin velocity magnitudes, respectively), Eqs. (3)–(6) can be simplified to yield:

$$-\frac{\partial p}{\partial x} + \eta \frac{\partial^2 u}{\partial z^2} = 0 \quad (3')$$

$$-\frac{\partial p}{\partial y} + \eta \frac{\partial^2 v}{\partial z^2} = 0 \quad (4')$$

$$\frac{\partial p}{\partial z} = 0 \quad (5')$$

$$\frac{\partial u}{\partial x} + \frac{\partial v}{\partial y} + \frac{\partial w}{\partial z} = 0 \quad (6')$$

Eqs. (3')–(6') are generally referred to as “two-dimensional lubrication-flow equations” in which the pressure variation in the  $z$ -direction is negligibly small. However, in contrast to the traditional lubrication models, the transverse velocity  $w$  (the velocity in the  $z$ -direction) is generally not zero (or constant) in the present case and, consequently, the last term on the left hand side of the continuity equation, Eq. (6'), does not vanish. Nevertheless, this term can be eliminated by integrating Eq. (6') in the  $z$ -direction to yield:

$$\int_{z_{\text{low}}}^{z_{\text{upp}}} \left( \frac{\partial u}{\partial x} + \frac{\partial v}{\partial y} \right) dz + w|_{z_{\text{upp}}} - w|_{z_{\text{low}}} = 0 \quad (7)$$

where  $z_{\text{upp}}(x, y)$  and  $z_{\text{low}}(x, y)$  are mathematical expressions for the upper and the lower surfaces of the channels and the associated transverse velocities,  $w|_{z_{\text{upp}}}$  and  $w|_{z_{\text{low}}}$ , are given by the appropriate boundary conditions discussed later.

### 2.2.2. Flow within the fiber tows

The resin flow through the fabric is described in the present work using the Darcy's law for an anisotropic porous medium as:

$$u = -\frac{1}{\eta} \left( K_{xx} \frac{\partial p}{\partial x} + K_{xy} \frac{\partial p}{\partial y} + K_{xz} \frac{\partial p}{\partial z} \right) \quad (8)$$

$$v = -\frac{1}{\eta} \left( K_{yx} \frac{\partial p}{\partial x} + K_{yy} \frac{\partial p}{\partial y} + K_{yz} \frac{\partial p}{\partial z} \right) \quad (9)$$

$$w = -\frac{1}{\eta} \left( K_{zx} \frac{\partial p}{\partial x} + K_{zy} \frac{\partial p}{\partial y} + K_{zz} \frac{\partial p}{\partial z} \right) \quad (10)$$

$$\frac{\partial u}{\partial x} + \frac{\partial v}{\partial y} + \frac{\partial w}{\partial z} = 0 \quad (11)$$

where  $K_{xx}$ ,  $K_{yy}$ ,  $K_{zz}$ ,  $K_{xy}=K_{yx}$ ,  $K_{xz}=K_{zx}$ , and  $K_{yz}=K_{zy}$  are the components of the symmetric tow permeability tensor.

Eqs. (8)–(11) can be simplified under the following assumptions: (a)  $K_{xx} = K_{yy} = K_{zz}$  and (b)  $K_{yz} = K_{zx} = 0$ . The first assumption is not typically fully justified since the longitudinal components of the permeability ( $K_{xx}$  and  $K_{yy}$ ) are generally larger (up to an order of magnitude) than the transverse component ( $K_{zz}$ ) of the permeability. However, this assumption greatly simplifies the computational procedure and, for simple fabric geometries, it is found, in the present work, that the results are different by only 1–2% relative to their more accurately determined counterparts corresponding to  $K_{xx}/K_{zz} = K_{yy}/K_{zz} = 10$ . The second assumption, on the other hand, is generally expected to be valid for at least two reasons: (a) for the orthogonal plain-weave architecture of the fabric, the material transverse principal direction is expected to be essentially coincident with the global  $z$ -axis; and (b) the second assumption is valid whenever the first assumption is valid. Again following the procedure of Simacek and Advani [7], which involves non-dimensionalization of the governing equations, and the use of the conditions:  $h/L \ll 1$  and  $WL/Uh \approx 1$ , Eqs. (8)–(11) become:

$$u = 0 \quad (8')$$

$$v = 0 \quad (9')$$

$$w = -\frac{K_{zz}}{\eta} \frac{\partial p}{\partial z} \quad (10')$$

$$\frac{\partial w}{\partial z} = 0 \quad (11')$$

Eqs. (8')–(11') indicate that the only non-zero component of the resin velocity within the fabric is the one in the  $z$ -direction and that, at given values of the in-plane  $x$ - and  $y$ -coordinates, this component of the velocity does not vary in the  $z$ -direction.

### 2.3. Boundary conditions

The following boundary conditions are used for the resin flow problem in the three regions:

- no slip ( $u = v = w = 0$ ) at the mold walls,  $z = \pm(h/2)$ ;
- at the fabric/channels contact surfaces,  $z_{\text{top}}$  and  $z_{\text{bot}}$ , the velocities and the pressure continuity are assumed, i.e.:

$$\phi(\text{in T})|_{z_{\text{top}}} = \phi(\text{in F})|_{z_{\text{top}}} \quad (12)$$

$$\phi(\text{in B})|_{z_{\text{bot}}} = \phi(\text{in F})|_{z_{\text{bot}}} \quad (13)$$

where  $\phi = p, u, v,$  or  $w$ .

It should also be noted that, as established in the previous section,  $u(\text{in F}) = v(\text{in F}) = 0$ . In addition, the definition of the ( $x$  and  $y$ ) in-plane boundary conditions is deferred until the final system of equations is derived (the next section).

### 2.4. The final system of equations

The resin velocities in the two channels can be obtained by integrating twice Eqs. (12) and (13), and using the boundary conditions given by Eqs. (12) and (13) to determine the integration constants. This procedure yields:

$$\left. \begin{aligned} u &= \frac{\partial p/\partial x}{\eta} \left( z - \frac{h}{2} \right) (z - z_{\text{top}}) \\ v &= \frac{\partial p/\partial y}{\eta} \left( z - \frac{h}{2} \right) (z - z_{\text{top}}) \end{aligned} \right\} \text{in regional T} \quad (14)$$

$$\left. \begin{aligned} u &= \frac{\partial p/\partial x}{\eta} \left( z + \frac{h}{2} \right) (z - z_{\text{bot}}) \\ v &= \frac{\partial p/\partial y}{\eta} \left( z + \frac{h}{2} \right) (z - z_{\text{bot}}) \end{aligned} \right\} \text{in region B} \quad (15)$$

The subsequent equations can be simplified by introducing the following expressions:  $h^{\text{T}}(x, y) = h/2 - z_{\text{top}}$ ,  $h^{\text{B}}(x, y) = z_{\text{bot}} - h/2$ ,  $h^{\text{F}}(x, y) = z_{\text{top}} - z_{\text{bot}}$ , which denote the height fields of the top channel and the bottom channels and the thickness field of the fabric, respectively.

Substitution of Eqs. (14) and (15) into the integrated form of the continuity equation, Eq. (7), for the two channels yields:

$$\begin{aligned} w^{\text{T}}|_{z=h/2} - w^{\text{T}}|_{z=z_{\text{top}}} \\ - \frac{1}{6\eta} \left( \frac{\partial((h^{\text{T}})^3(\partial p^{\text{T}}/\partial x))}{\partial x} + \frac{\partial((h^{\text{T}})^3(\partial p^{\text{T}}/\partial y))}{\partial y} \right) = 0 \end{aligned} \quad (16)$$

$$\begin{aligned} w^{\text{B}}|_{z=z_{\text{bot}}} - w^{\text{B}}|_{z=-h/2} \\ - \frac{1}{6\eta} \left( \frac{\partial((h^{\text{B}})^3(\partial p^{\text{B}}/\partial x))}{\partial x} + \frac{\partial((h^{\text{B}})^3(\partial p^{\text{B}}/\partial y))}{\partial y} \right) = 0 \end{aligned} \quad (17)$$

where superscripts T and B are used to denote the quantities pertaining to the top and the bottom channels.

The first two terms on the left hand side of Eqs. (16) and (17) are defined by the boundary conditions discussed earlier as:

$$w^{\text{T}}|_{z=h/2} = 0 \quad (18)$$

$$w^{\text{T}}|_{z=z_{\text{top}}} = \frac{K_{zz}(p^{\text{B}} - p^{\text{T}})}{\eta h^{\text{F}}} \quad (19)$$

$$w^{\text{B}}|_{z=-h/2} = 0 \quad (20)$$

$$w^{\text{B}}|_{z=z_{\text{bot}}} = \frac{K_{zz}(p^{\text{B}} - p^{\text{T}})}{\eta h^{\text{F}}} \quad (21)$$

Consequently Eqs. (16) and (17) can be rewritten as

$$\begin{aligned} - \frac{K_{zz}(p^{\text{B}} - p^{\text{T}})}{\eta h^{\text{F}}} \\ - \frac{1}{6\eta} \left( \frac{\partial((h^{\text{T}})^3(\partial p^{\text{T}}/\partial x))}{\partial x} + \frac{\partial((h^{\text{T}})^3(\partial p^{\text{T}}/\partial y))}{\partial y} \right) = 0 \end{aligned} \quad (22)$$

$$\begin{aligned} \frac{K_{zz}(p^{\text{B}} - p^{\text{T}})}{\eta h^{\text{F}}} \\ - \frac{1}{6\eta} \left( \frac{\partial((h^{\text{B}})^3(\partial p^{\text{B}}/\partial x))}{\partial x} + \frac{\partial((h^{\text{B}})^3(\partial p^{\text{B}}/\partial y))}{\partial y} \right) = 0 \end{aligned} \quad (23)$$

Eqs. (22) and (23) represent the final system of equations consisting of two coupled linear elliptic partial differential equations with the pressures  $p^{\text{T}}$  and  $p^{\text{B}}$  as dependent variables. To solve these equations, boundary conditions along the ( $x$ - $y$ ) in-plane boundaries of the unit cell must be prescribed. For the un-sheared balanced plain-weave fabric architecture in which the unit cell boundaries are the lines of geometrical symmetry, a fixed pressure gradient can be enforced in one principal direction while requiring periodicity in the pressure distribution in the direction normal to the direction in which the pressure gradient is prescribed. This type of boundary conditions is generally used since it enables determination of the off-diagonal ( $K_{xy}$ ,  $K_{yz}$  and  $K_{xz}$ ) components of the effective preform permeability tensor. A more detailed discussion of the in-plane boundary conditions is given later in the context of the effect of fabric shearing on the choice of in-plane boundary conditions.

The final system of partial differential equations, Eqs. (22) and (23), contains the thickness fields:  $h^{\text{T}}(x, y)$ ,  $h^{\text{B}}(x, y)$  and  $h^{\text{F}}(x, y)$ . These fields are defined in the present work using the analytical expressions for the top and the bottom surfaces of the fabric preform (Eqs. (1) and (2)). These expressions are generally considered as reasonably good approximations of the actual orthogonal plain-weave fabric architecture with a near elliptical cross-section area. It should be noted, however, that over-simplification of the fabric architecture (e.g. using square or circularly shaped tows) may lead to erroneous results and must be avoided. In general, the thickness fields can be constructed using direct experimental measurements such as quantitative metallographic

analysis of consolidated and sectioned parts, e.g. [11], and through the use of computerized image analysis of the fabric surface, e.g. [12]. The second of these two methods is quite appealing since the image conversion procedure can be directly coupled with the solution scheme for Eqs. (22) and (23).

Due to complexity in the  $h^T(x, y)$ ,  $h^B(x, y)$  and  $h^F(x, y)$  functions, Eqs. (22) and (23), cannot be solved analytically. However, finding the numerical solution to Eqs. (22) and (23) is relatively straightforward. In the present work, MATLAB general-purpose mathematical package [10] and a finite difference method are used to solve Eqs. (22) and (23).

Once Eqs. (22) and (23) are solved, the resulting pressure fields can be used, in conjunction with Eqs. (14) and (15), to compute the corresponding in-plane velocity fields in the two channels. Integration of these velocity fields over the side boundaries of the quarter unit cell then enables determine of the total resin flow rate,  $Q = [Q_x, Q_y]$ , through the quarter unit cell in the two principal direction. The components of the effective in-plane preform permeability,  $K_{xx}^{eff}$ ,  $K_{yy}^{eff}$  and  $K_{xy}^{eff}$  are then computed using the two-dimensional Darcy’s law and the known imposed values of the pressure gradient.

2.5. Application of the model to the multi-layer fabric

The model developed thus far pertains to a single-layer fabric preform. In typical RTM and VARTM processes, the preforms may contain several fabric layers. In such multi-layer preforms, nesting and compaction generally have a significant effect and must be included when predicting preform permeability. Numerous experiments, e.g. [13,14], confirmed that permeability varies with a number of layers.

The single-layer model developed in the previous section can be readily extended to a multi-layer preform. A schematic of two types of two-layer plain-weave fabric preforms is given in Fig. 3(a) and (b). The two types are generally referred to as “in-phase” and “out-of-phase” fabric architectures or laminates. In the case of an  $n$ -layer fabric preform, if the channels are labeled using consecutive integers (with the bottom channel being denoted as channel “1”), the analytical procedure for a single-layer fabric preform used in the previous section yields  $(n + 1)$  coupled elliptical partial differential equations with  $n + 1$  unknown pressures  $p^{(1)}, p^{(2)}, \dots, p^{(n+1)}$  as:

$$-\frac{K_{zz}}{\eta h^{F_1}}(p^{(2)} - p^{(1)}) - \frac{1}{6\eta} \nabla((h^{(1)})^3 \nabla p^{(1)}) = 0 \quad (24)$$

$$\frac{K_{zz}}{\eta h^{F_{i-1}}}(p^{(i)} - p^{(i+1)}) - \frac{K_{zz}}{\eta h^{F_i}}(p^{(i+1)} - p^{(i)}) - \frac{1}{6\eta} \nabla((h^{(i)})^3 \nabla p^{(i)}) = 0, \quad i = 2, 3, \dots, n \quad (25)$$

$$\frac{K_{zz}}{\eta h^{F_n}}(p^{(n+1)} - p^{(n)}) - \frac{1}{6\eta} \nabla((h^{(n+1)}) \nabla p^{(n+1)}) = 0 \quad (26)$$

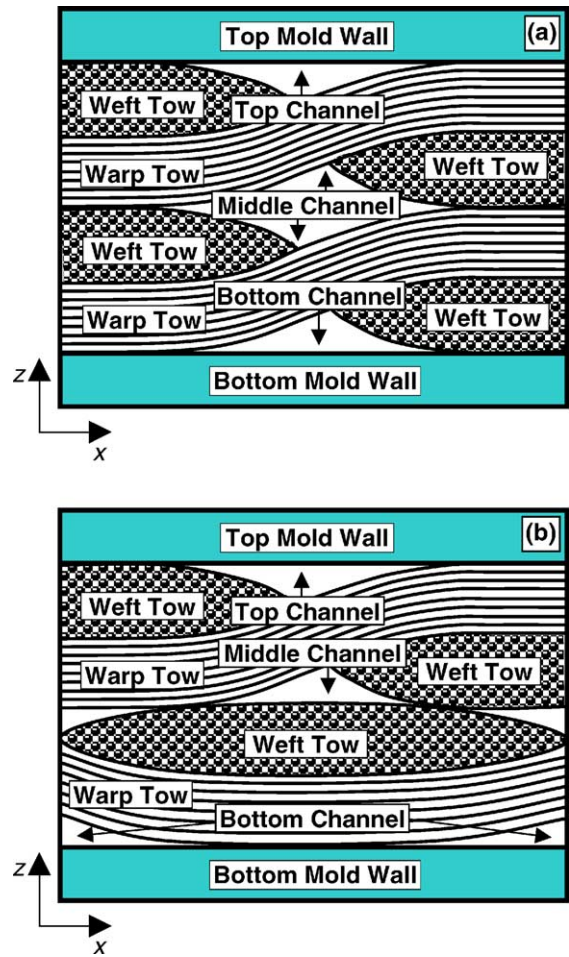


Fig. 3.  $x$ - $z$  section of a quarter of the unit cell for (a) an in-phase and (b) an out-of-phase two-layer orthogonal plain-weave fabric.

where  $h^{F_i}$  ( $i = 1, \dots, n$ ) denotes the thicknesses of the  $i$ th fabric layer (numbered starting from the bottom of the mold) and  $h^{(i)}$  ( $i = 1, \dots, n + 1$ ) are the heights of the inter-fabric or tool/fabric resin channels (also numbered starting from the bottom of the mold). The system of equations defined by Eqs. (24)–(26) is solved using the same computational procedure used for the one-layer fabric preform.

2.6. Shear-induced fiber volume fraction correction for permeability

When the fabric is sheared in the  $x$ -direction, as shown in Fig. 7(b), weft tows are rotated but remain stress free. Consequently, the dimension of the fabric-preform unit cell in the  $y$ -direction is altered causing a change in the effective fiber volume fraction in the unit cell. This change in the fiber volume fraction can have a significant effect on preform permeability at large shear angles and, hence, must be taken into account. The procedure described below is used to correct permeabilities in the sheared fabrics obtained using the original model of Simacek and Advani [7] as reviewed in Sections 2.4 and 2.5.

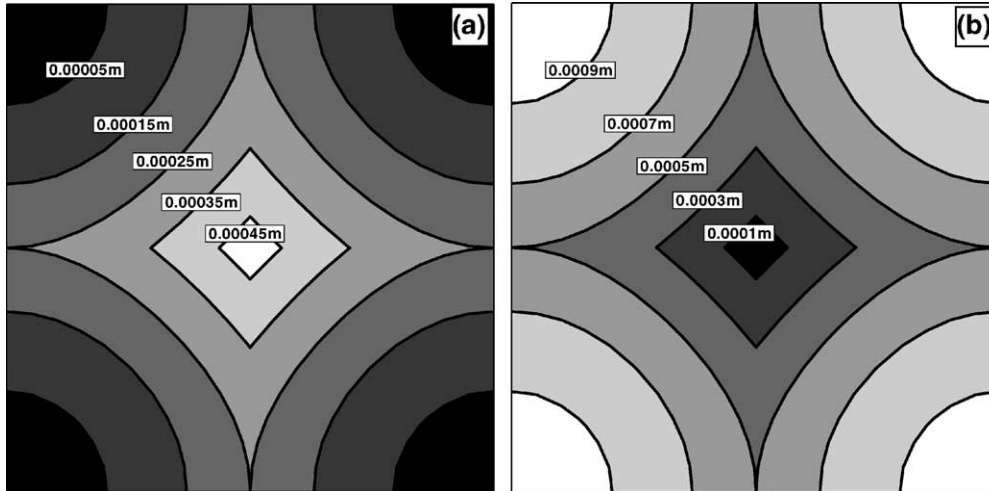


Fig. 4. (a) Resin channels height and (b) fabric thickness fields in an un-sheared one-layer orthogonal plain-weave fabric preform.

To quantify the permeability correction described above, the Kozeny-Carman relation, e.g. [20], for permeability of the porous media with a fibrous architecture is used. According to this relation, permeability of such media is given by:

$$K = \frac{r^2(1 - f)^3}{cf^2} \quad (27)$$

where  $r$  and  $f$  are the fiber radius and the fiber volume fraction, respectively, while  $c$  is a fibrous-medium architecture-dependent constant.

When the fabric preform is sheared in the  $x$ -direction by an angle  $\theta$ , the fiber volume fraction in fabric tows changes as:

$$f_\theta = \frac{f_0}{\sin(90 - \theta)} \quad (28)$$

where the angle  $\theta$  is given in degrees and the subscripts 0 and  $\theta$  are used to denote the value of a respective quantity in the un-sheared fabric and in the fabric sheared by an angle  $\theta$ , respectively.

To account for a shear-induced change in the fiber volume fraction, the permeability values for sheared fabric preforms obtained using the models described in Sections 2.4 and 2.5, should be multiplied by the following correction factor:

$$K_{\text{corr}} = \frac{f_0^2(1 - f_\theta)^3}{(1 - f_0)^3 f_\theta^2} \quad (29)$$

### 3. Results and discussion

#### 3.1. Un-sheared single-layer plain-weave fabric preforms

The model developed in Section 2.4 is used in this section to analyze the pressure distribution within the un-sheared single-layer balanced orthogonal plain-weave quarter unit

cell. Due to the symmetry of the unit cell with respect to the  $z = 0$  plane, the pressure distributions within the top and the bottom resin channels are identical and, hence, there is no transverse flow of the resin through the fabric preform. Also, as established in Section 2.4, there is no variation of the pressure in the  $z$ -direction within the channels. The variation of the top- and bottom-channel heights and of the fabric thickness in the  $x$ - $y$  plane within a quarter unit cell, used as input in the present analysis, are shown in Fig. 4(a) and (b), respectively. The variation of the pressure in the  $x$ - $y$  plane within the resin channels of a quarter unit cell for the fixed pressure drop of  $1.0 \times 10^5$  in the  $x$ -direction is shown in Fig. 5. The pressure distribution (or more precisely its

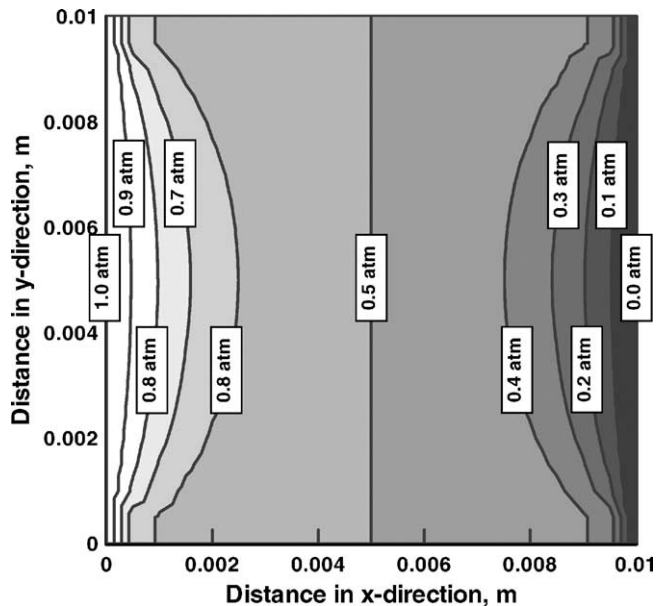


Fig. 5. Pressure distribution in the  $x$ - $y$  plane within a resin channel in the case of an un-sheared single-layer balanced orthogonal plain-weave fabric preform.

gradient) at a given  $x$ - $y$  location correlates inversely with the local height of the resin channel in order to satisfy the continuity equation. It should be also noted that due to the symmetry of the fabric geometry with respect to the quarter unit cell boundaries normal to the  $y$ -direction, zero-flux (i.e. zero pressure gradient) conditions are found in the  $y$ -direction at these boundaries.

### 3.2. Effect of the number of layers in un-sheared plain-weave fabric preforms

The model developed in Section 2.5 is used in the present section to predict permeability of the balanced un-sheared single- and multi-layer orthogonal plain-weave fabric architectures. In all the calculations carried out in this section, as well as in the calculations carried out in the previous section, the following unit cell parameter and one-layer fabric thickness values are used:  $L_1 = L_2 = L = 0.01$  m and  $h = 0.001$  m. Also the transverse permeability of the fiber tows is set to a typical (fixed) value,  $K_{zz} = 1 \times 10^{-10}$  m<sup>2</sup>.

To determine the effect of the number of fabric layers on the effective permeability, the model developed in the previous section is used for the cases of 1-, 2-, 3-, 5-, 10- and 20-layer in-phase orthogonal balanced plain-weave fabric preforms in the absence of layer nesting. The results of this calculation are presented in Fig. 6. These results show that as the number of layers increases, the permeability rises but at an ever decreasing rate so that in fabric preforms with 10 or more layers, the effect of the number of layers on permeability becomes insignificant. This finding can be easily rationalized by recognizing that as the number of layers in the fabric increases, the effect of the bottom and the top resin channels which are more restrictive to the fluid flow (and thus reduce effective preform permeability) decreases.

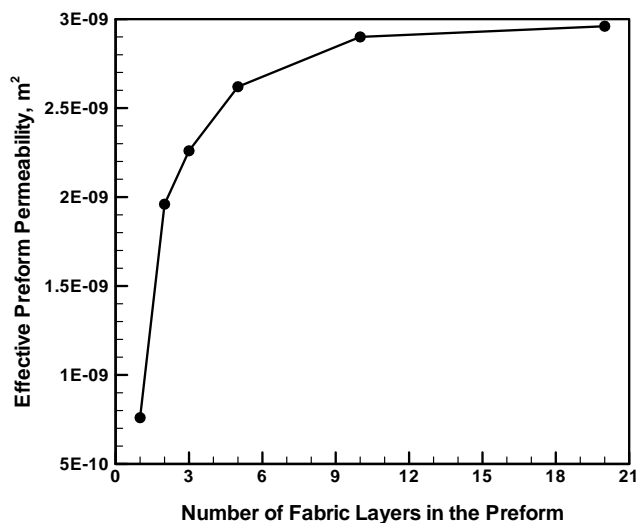


Fig. 6. The effect of the number of fabric layers on the effective permeability of an un-sheared balanced plain-weave fabric preform.

### 3.3. Effect of fabric shear on permeability

As pointed out earlier, when the fabric preform is forced to conform to the ridges and recesses of a mold, it may locally undergo shear deformation. Such deformation can significantly affect local permeability of the preform. As shown in Fig. 7, when a balanced square-cell plain-weave fabric is sheared, two important factors must be considered: (a) the unit cell size increases and to make the calculations of preform permeability manageable, the shear angle  $\alpha = \tan^{-1}(m/n)$  is generally allowed to take only the values corresponding to relatively small integers  $m$  and  $n$ ; and (b) the boundaries of the unit cell, unlike the case of the initial square-shape unit cell, are no longer the lines of symmetry of the fabric structure. Consequently, the boundary conditions imposed along the boundaries of the unit cell have to be modified relative to those used in the case of the un-sheared unit cell. For instance, if a fixed pressure drop is applied in the  $x$ -direction, the symmetry conditions along the unit cell boundaries normal to the  $y$ -coordinate require that zero pressure-gradient boundary conditions be applied in the  $y$ -direction. In the case of a sheared fabric preform, on the other hand, the unit cell boundaries normal to the  $y$ -direction are not any longer the lines of symmetry of the fabric architecture and, hence, only the periodic boundary condition (the corresponding pressure values along the two

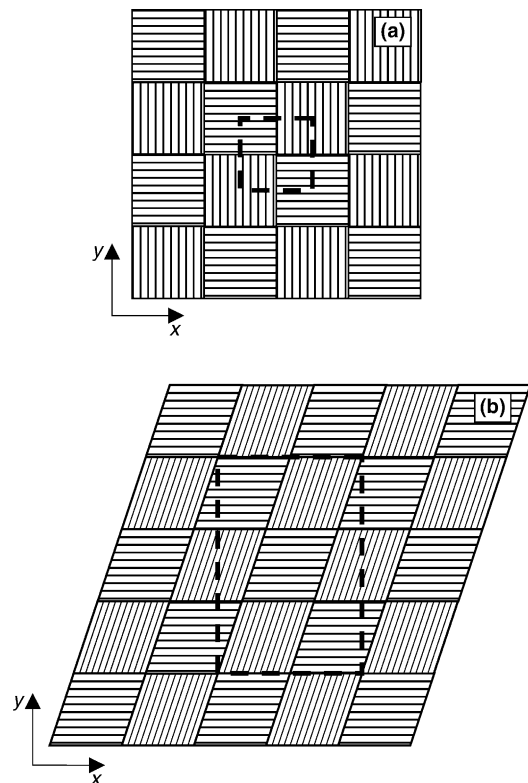


Fig. 7. Effect of fabric shearing on the size of the quarter unit cell (denoted using heavy dashed lines) in balanced plain-weave fabric architectures: (a) un-sheared fabric; (b) fabric sheared by an angle  $\alpha = \tan^{-1}(1/3)$  in the  $x$ -direction.

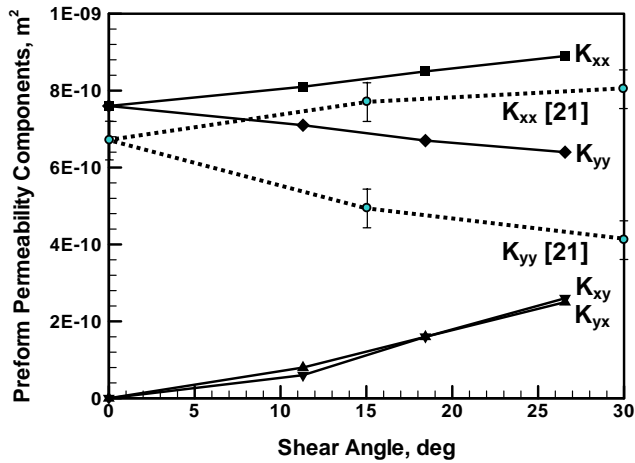


Fig. 8. The effect of shear on permeability of a single-layer balanced orthogonal plain-weave fabric preform.

unit-cell boundaries normal to the  $y$ -direction are identical) can be applied.

The effect of shear deformation (measured by the magnitude of the shear angle  $\alpha$ ) on the effective permeability of single-layer plain-weave fabric preforms is displayed in Fig. 8. An example of the variation of the top- and bottom-channel heights and of the fabric thickness in the  $x$ - $y$  plane within a quarter unit cell, used as input in the present analysis, are shown in Figs. 9(a) and (b), respectively. For comparison, the experimental values of preform permeabilities obtained in Ref. [8] are also shown in Fig. 8. While the agreement between the corresponding computational and the experimental values is only fair, the effect of shear deformation on preform permeability appears to be quite well predicted by the model. In addition, the corresponding computed values of the in-plane off-diagonal ( $K_{xy}$  and  $K_{yx}$ ) elements of the effective permeability are very close as required by symmetry of the orthogonal plain-weave fabric architecture.

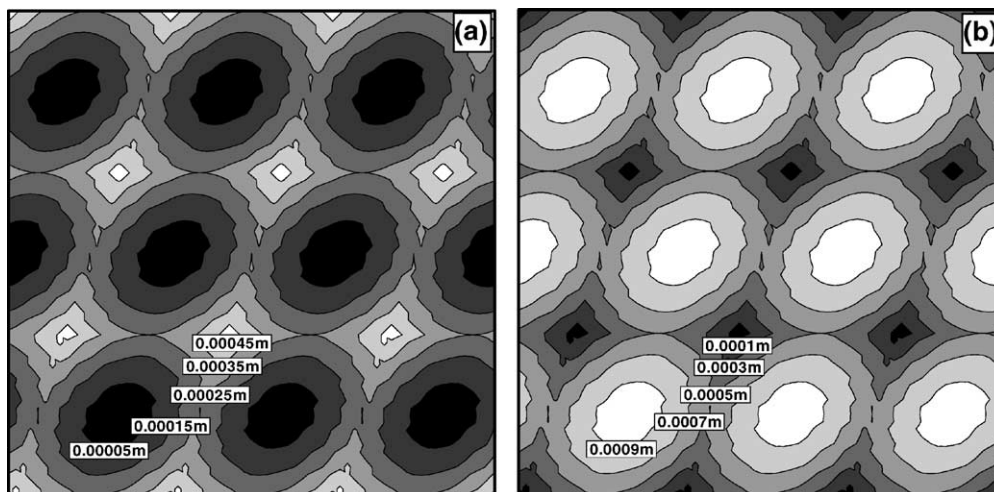


Fig. 9. (a) Resin channels height and (b) fabric thickness fields in a one-layer orthogonal plain-weave fabric preform subjected to shear in the  $x$ -direction by an angle of  $\alpha = \tan^{-1}(1/3)$ .

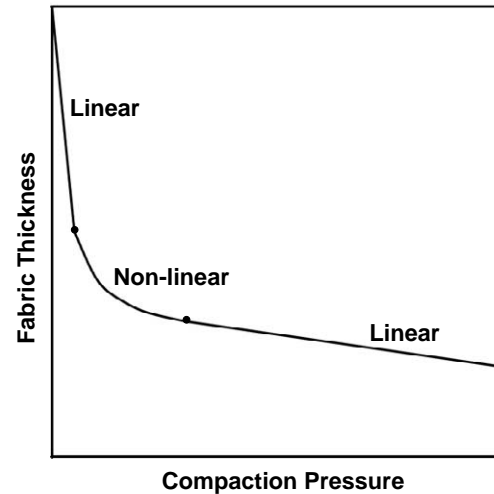


Fig. 10. A typical compaction-pressure vs. preform-thickness curve for a plain-weave fabric architecture.

### 3.4. Effect of preform compaction on permeability

When the fabric is subjected to compression during mold closing in the RTM process or during evacuation of the vacuum bag in the VARTM process, it undergoes a number of changes such as: the cross-section of the fiber tow flattens, the pores and gaps between the fibers inside tows as well as between individual tows are reduced, the tows undergo elastic deformation, inter-layers shifting (nesting), etc. A typical compression-pressure versus preform thickness curve for a woven fabric is depicted in Fig. 10 [15]. The curve shown in Fig. 10 has three distinct parts: two linear and one nonlinear. In the low-pressure linear and the nonlinear portions of the pressure versus thickness curve, preform compaction is dominated by a reduction of the pore and the gap sizes between the fibers in tows. In the high-pressure linear region of the pressure versus thickness curve, on the other hand, preform

compaction involves mainly tow bending and nesting. Typical liquid molding processes such as RTM or VARTM involve pressures which correspond to the high-pressure linear pressures versus thickness region. Hence, the effect of fabric compaction on permeability of the fabric preform associated with the high-pressure linear compaction regime is investigated in this section.

To quantify the effect of preform compaction (in the high-pressure linear region) on permeability of the balanced orthogonal plain-weave fabric, the beam-bending-based micro-mechanical model developed in a series of papers by Chen and Chou [16–18] is utilized in the present work. The model of Chen and Chou [16–18] is based on a number of well-justified assumptions such as: (a) the fabric is considered to extend indefinitely in the  $x$ - $y$  plane and, hence, can be represented using the unit cells such as the one shown in Fig. 2; (b) tows in the fabric are treated as a transversely isotropic solid material; (c) the fabric is subjected to the compaction pressure only in the through-the-thickness direction, and can freely adjust its shape in the  $x$ - $y$  plane; (d) since the compaction analyzed corresponds to the high-pressure linear region, no voids or gaps are assumed to exist between the fibers in tows or between the tows; (e) during fabric compaction, the cross-section area of the tows is assumed to remain unchanged but the shape of the cross-section undergoes a change; and (f) as compaction proceeds, the deformation of the tows leads to an increase in the effective volume fraction of the fibers in the fabric and, in the limit of complete compaction of the tows, the volume fraction of the fibers in the fabric becomes equal to that in the individual tows.

In order to derive a relationship between the reduction in the fabric thickness, the effective volume fraction of the fibers and various distributions and magnitudes of the applied compaction pressure, Chen and Chou [16–18] applied a simple procedure from the solid mechanics beam theory. Toward that end, the one-quarter unit cell shown in Fig. 2 is first simplified by replacing the two warp and the two weft tows with four beams. Next based on the symmetry of the simplified model, it is shown that the problem can be further simplified using a single beam and the appropriate distribution of the applied and contacting pressures (Fig. 11). The model of Chen and Chou [16–18] is utilized in the present work to compute the effect of the compaction pressure on the channel heights ( $h^T(x, y)$  and  $h^B(x, y)$ ) and on the fabric thickness,  $h^F(x, y)$  fields. These fields are, in turn, used in the lubrication model presented in the Section 2.4 to quantify the effect of fabric compaction on the effective permeability of a one-layer orthogonal plain-weave fabric.

The effect of the compaction force applied to the upper and the lower (rigid and flat) molds on the effective permeability of a one-layer orthogonal plain-weave fabric is displayed in Fig. 12. In these calculations, the Young's modulus is assigned a value of 22 GPa and a sinusoidal distribution of the applied and the contacting pressures is assumed [18]. An example of the variation of the top- and the bottom-channel

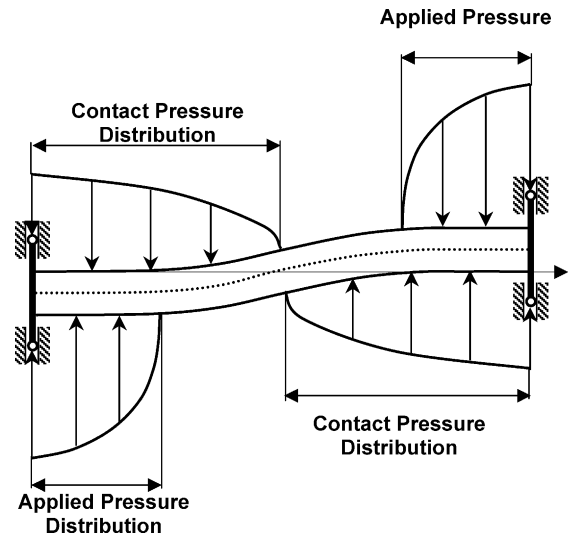


Fig. 11. A schematic of the pressure distribution on a curved beam used in the calculation of permeability of un-sheared one-layer orthogonal plain-weave fabrics.

heights and of the fabric thickness in the  $x$ - $y$  plane within a quarter unit cell, used as input in the present analysis, are shown in Fig. 13(a) and (b), respectively. For comparison, the experimental results reported by Sozer et al. [19] are also shown in Fig. 12. It is seen that a reasonably good agreement exists between the both the magnitude of the predicted preform permeability and its change with the applied compaction force.

### 3.5. Effect of layer nesting

As mentioned earlier shifting of fabric layers followed by their more compact packing (the phenomenon generally referred to as layers “nesting”) can have a major effect on the effective fiber density in the preform and, hence, on

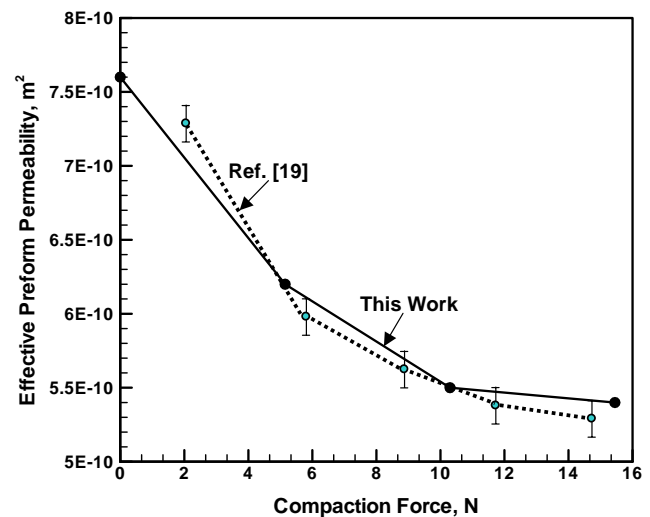


Fig. 12. Effect of compaction (represented by the magnitude of the compaction force) on permeability of a one-layer un-sheared orthogonal plain-weave fabric preform.

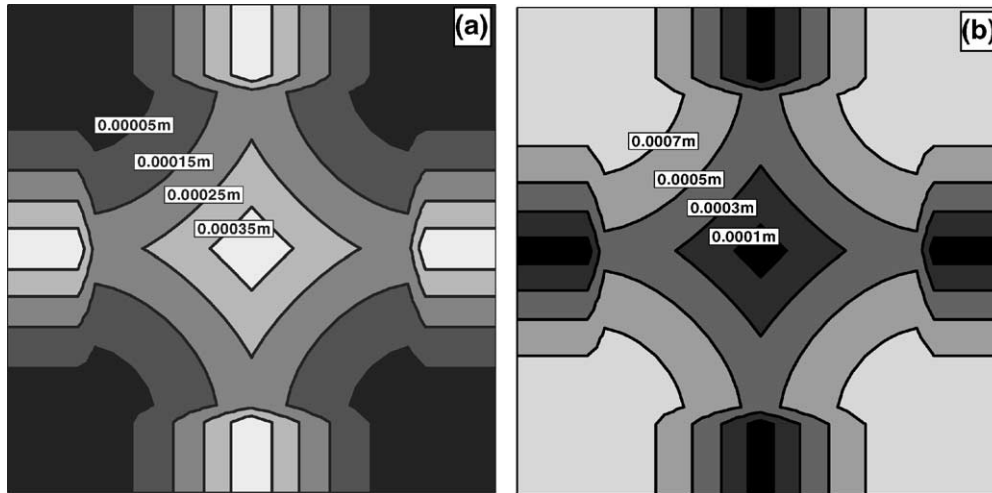


Fig. 13. (a) Resin channels height and (b) fabric thickness fields in an un-sheared one-layer orthogonal plain-weave fabric preform subject to a total compressive force of 10.3N via rigid, flat upper and lower tool surfaces.

permeability of the preform. Nesting of the fabric layers can particularly take place under high applied pressures which are sufficient to overcome inter-tow friction. The thickness reduction in balanced orthogonal plain-weave fabrics whose geometry is represented by Eqs. (1) and (2), due to layers nesting, has been analyzed by Ito and Chou [9] who derived the following relation for the fabric thickness reduction caused by nesting:

$$\Delta h^{\text{nesting}} = h \begin{cases} 2 - \cos \frac{\phi_x}{2} - \cos \frac{\phi_y}{2}, & |\phi_x| \leq \frac{\pi}{2}, |\phi_y| \leq \frac{\pi}{2}, \\ 2 - \sin \frac{|\phi_x|}{2} - \cos \frac{\phi_y}{2}, & \frac{\pi}{2} \leq |\phi_x| \leq \pi, |\phi_y| \leq \frac{\pi}{2}, \\ 2 - \cos \frac{\phi_x}{2} - \sin \frac{|\phi_y|}{2}, & |\phi_x| \leq \frac{\pi}{2}, \frac{\pi}{2} \leq |\phi_y| \leq \pi, \\ 2 - \sin \frac{|\phi_x|}{2} - \sin \frac{|\phi_y|}{2}, & \frac{\pi}{2} \leq |\phi_x| \leq \pi, \frac{\pi}{2} \leq |\phi_y| \leq \pi, \end{cases} \quad (30)$$

where  $\phi_x = (2\pi/L)s_x$  and  $\phi_y = (2\pi/L)s_y$  are dimensionless while  $s_x$  and  $s_y$  are the dimensional relative shifts of the adjacent layers in the  $x$ - and  $y$ -directions, respectively.

Two non-nesting cases associated with zero nesting, reduction in the fabric thickness can be identified: (a)  $\phi_x = \phi_y = 0$  which corresponds to the iso-phase laminate case and (b)  $\phi_x = \phi_y = \pm(\pi/2)$  corresponding to the out-of-phase laminate case.

The relations given in Eq. (30) are used in the present work to examine the effect of layers nesting on fabric permeability. While, in general, fabric compaction during the high-pressure linear compaction stage can involve both elastic distortions (tow bending) and layers nesting, the two modes of fabric compaction are generally considered as decoupled and can be considered separately.

The effect of nesting (quantified by the magnitudes of the dimensionless layer shifts in the  $x$ - and the  $y$ -directions,  $\phi_x$  and  $\phi_y$ , respectively) in a two-layer orthogonal plain-weave fabric is shown in Fig. 14. The values displayed pertain to the ratio of fabric permeability at the given values of  $\phi_x$  and  $\phi_y$

and fabric permeability at  $\phi_x = \phi_y = 0$ . As expected, fabric nesting gives rise to the reduction in fabric permeability. Furthermore, for the case of a out-of-phase laminate fabric ( $\phi_x = \phi_y = \pm(\pi/2)$ ), fabric permeability is only about 30% of its value in the in-phase laminate fabric. This finding is in excellent agreement with its experimentally counterpart reported by Sozer et al. [19].

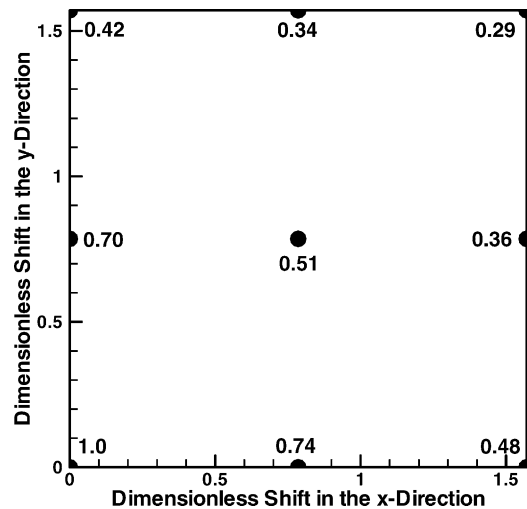


Fig. 14. The effect of nesting on the ratio of fabric permeability at the given values of layer shifts in the  $x$ - and  $y$ -directions and fabric permeability of an un-nested in-phase laminate fabric.

#### 4. Conclusions

Based on the results obtained in the present work, the following main conclusions can be drawn:

1. Effective permeability of the orthogonal plain-weave fabric preforms can be determined computationally by combining a lubrication model for the resin flow through tool-surface/fabric-tow and tow/tow channels with the Darcy's law for the resin flow through the fabric tows.
2. The computational approach presented in this work enables assessment of the contribution that various phenomena such as the mold walls, fabric shearing, interlayer shifting and restacking as well as fabric compaction due to the infiltration pressure make to orthogonal plain-weave fabric-preform permeability.
3. While no comprehensive set of experimental data is available to fully test validity of the present model, the agreement of the model predictions with selected experimental results can be generally qualified as reasonable.

#### Acknowledgements

The material presented in this paper is based on work supported by the US Army Grant Number DAAD19-01-1-0661. The authors are indebted to Drs. Walter Roy, Fred Stanton, William DeRosset and Dennis Helfritsch of ARL for the support and a continuing interest in the present work. The authors also acknowledge the support of the Office of High Performance Computing Facilities at Clemson University.

#### References

- [1] L.J. Lee, Liquid composite molding, in: T.G. Gutowski (Ed.), *Advanced Composites Manufacturing*, Wiley, New York, 1997, pp. 393–456.
- [2] R.C. Lam, J.L. Kardos, The permeability and compressibility of aligned and cross-piled carbon-fiber beds during processing of composites, in: *Proceedings of the Third Technological Conference of American Society for Composites*, 1988.
- [3] T.G. Gutowski, Consolidation experiments for laminate composites, *SAMPE Q.* 4 (1985) 221.
- [4] B.R. Gebart, Permeability of unidirectional reinforcement for RTM, *J. Compos. Mater.* 26 (1992) 1100.
- [5] S. Ranganathan, F. Phelan, S.G. Advani, A generalized model for the transverse permeability of unidirectional fibrous media, *Polym. Compos.* 17 (1996) 222.
- [6] S. Ranganathan, G.M. Wise, F.R. Phelan, R.S. Parnas, S.G. Advani, A numerical and experimental study of the permeability of fiber preforms, in: *Proceedings of the 10th ASM/ESD Advanced Composites Conference*, October 1994.
- [7] P. Simacek, S.G. Advani, Permeability model for a woven fabric, *Polym. Compos.* 17 (1996) 887.
- [8] F.D. Dungan, M.T. Senoguz, A.M. Sastry, D.A. Faillaci, Simulations and experiments on low-pressure permeation of fabrics. I. 3D modeling of unbalanced fabric, *J. Compos. Mater.* 35 (2001) 1250.
- [9] M. Ito, T.W. Chou, An analytical and experimental study of strength and failure behavior of plain weave composites, *J. Compos. Mater.* 32 (1998) 2.
- [10] MATLAB, 6th ed., *The Language of Technical Computing*, The MathWorks Inc., Natick, MA, 2000.
- [11] P. Falzon, V.M. Karbhari, Effects of Compaction on the Stiffness and Strength of Plain Woven Composites, draft of paper.
- [12] K.F. Heitzmann, Determination of in-plane permeability of woven and non-woven fabrics, Master's Thesis, University of Illinois at Urbana-Champaign, 1994.
- [13] N. Pearce, J. Summerscales, The compressibility of a reinforcement fabric, *Compos. Manuf.* 6 (1995) 15.
- [14] R.A. Saunders, C. Lekakou, M.G. Bader, Compression and microstructure of fiber plain woven cloths in the processing of polymer composites, *Compos. Part A* 29A (1998) 443.
- [15] J. Hu, A. Newton, Low-load lateral-compression behavior of woven fabrics, *J. Text Inst. Part I* 88 (1997) 242.
- [16] B. Chen, T.W. Chou, Compaction of woven-fabric preforms in liquid composite molding processes: single-layer deformation, *Compos. Sci. Technol.* 59 (1999) 1519.
- [17] B. Chen, T.W. Chou, Multi-layer deformation, *Compos. Sci. Technol.* 60 (2000) 2223.
- [18] B. Chen, E.J. Lang, T.W. Chou, Experimental and theoretical studies of fabric compaction behavior in resin transfer molding, *Mater. Sci. Eng. A* 317 (2001) 188.
- [19] E.M. Sozer, B. Chen, P.J. Graham, S. Bickerton, T.W. Chou, S.G. Advani, Characterization and prediction of compaction force and preform permeability of woven fabrics during the resin transfer molding process, in: *Proceedings of the Fifth International Conference on Flow Processes in Composite Materials*, Plymouth, UK, 12–14 July 1999, pp. 25–36.
- [20] F.D. Dungan, M.T. Senoguz, A.M. Sastry, D.A. Faillaci, On the use of darcy permeability in sheared fabrics, *J. Reinforced Plast. Compos.* 18 (1999) 472.